This is the Pre-Published Version.

This version of the article has been accepted for publication, after peer review (when applicable) and is subject to Springer Nature's AM terms of use(https://www.springernature.com/gp/open-research/policies/accepted-manuscript-terms), but is not the Version of Record and does not reflect post-acceptance improvements, or any corrections. The Version of Record is available online at: http://dx.doi.org/10.1007/s10237-020-01380-x.

Numerical study on the adhesion of a circulating tumor cell in a curved microvessel

Jingyu Cui[1], Yang Liu[1*], Lanlan Xiao[2], Shuo Chen[3], Bingmei M. Fu[4]

[1]Research Centre for Fluid‐Structure Interactions, Department of Mechanical Engineering, The Hong Kong Polytechnic University, Hung Hom, Hong Kong, China

[2]School of Mechanical and Automotive Engineering, Shanghai University of Engineering Science, Shanghai, China

[3]School of Aerospace Engineering and Applied Mechanics, Tongji University, Shanghai, China

[4]Department of Biomedical Engineering, The City College of the City University of New York, New York City, USA

Abstract

The adhesion of a circulating tumor cell (CTC) in a three-dimensional curved microvessel was numerically investigated. Simulations were first performed to characterize the differences in the dynamics and adhesion of a CTC in the straight and curved vessels. After that, a parametric study was performed to investigate the effects of the applied driven force density f (or the flow Reynolds number Re) and the CTC membrane bending modulus K_b on the CTC adhesion. Our simulation results show that the CTC prefers to adhere to the curved vessel as more bonds are formed around the transition region of the curved part due to the increased cell-wall contact by the centrifugal force. The parametric study also indicates that when the flow driven force f (*or* Re) increases or when the CTC becomes softer (K_b decreases), the bond formation probability increases and the bonds will be formed at more sites of a curved vessel. The increased f (or Re) brings a larger centrifugal force while the decreased K_b generates more contact areas at the cell-wall interface, both of which are beneficial to the bond formation. In the curved vessel, it is found that the site where bonds are formed the most (hotspot) varies with the applied f and the K_b. For our vessel geometry, when f is small, the hotspot tends to be within the first bend of the vessel; while as f increases or K_b decreases, the hotspot may shift to the second bend of the vessel.

Keywords: cell adhesion, dissipative particle dynamics, curved microvessel, circulating tumor cell

1. Introduction

The most dangerous aspect of cancer is its ability to metastasize. During metastasis, tumor cells detach from the primary tumor and invade either the blood circulatory or lymphatic system, in which they can be transported to a new site and proliferate there to form a new tumor. Ideally, blocking tumor cell adherence to vessels, one important step in the cancer metastatic cascade, can be a new tumor therapy strategy which requires deeper insight into this metastatic process. Circulating tumor cells (CTCs) have been demonstrated to play a key role in tumor metastasis (Poudineh et al. 2016). During the metastasis, the majority of the CTCs are trapped and lethally damaged in the microvasculature when they circulate to the distant target organs, leading to cell death and 'metastatic inefficiency' (Weiss 1990; Mook et al., 2003). To successfully colonize in a distant organ, the CTCs must first adhere to the endothelial cells that form the wall of the microvessels, specifically, the post-capillary venules (Cai et al., 2012; Guo et al, 2014), then transmigrate to the surrounding tissue through the endothelial barrier (extravasation), and eventually survive in the foreign environment of the metastatic organs. The circulation of the blood plays a significant role in determining where the CTCs go. CTCs usually get trapped in the first set of the capillaries that they encounter downstream from the point of entry due to the size restriction (Weiss 1990; Guo et al, 2014). Guo et al (2014) found that compared to only ~3% of the circulating rigid beads, ~42% of the circulating flexible breast cancer cells escape the capillary trap and arrest and adhere in the post-capillary venules. The adhesion of the CTCs to the post-capillary venules is a principal step in the cancer metastasis that has attracted tremendous attention in the past few decades, as understanding this step may lead to new therapeutic concepts for tumor metastasis. A detailed review of the adhesion of CTCs to the microvessel wall under hydrodynamic conditions can be found in (Haier and Nicolson 2001) and a more recent review on cell adhesion in cancer can be found in (Janiszewska et al. 2020).

One big progress achieved about the cell adhesion is the recognition of receptor-ligand bonds for mediating the adhesive dynamics of cells (Zhu et al. 2000, Bao et al, 2010). A successful cell arrest/adhesion relies on the competition between adhesive and anti-adhesive forces, and the rates at which the bonds are formed and ruptured (Weiss 1992). Moreover, this complex adhesion process depends on the local microenvironment in the metastatic organ, including the geometric features of

the vasculature, the local hemodynamic factors (Wirtz et al. 2011), the cytokines and other circulating factors that activate the cell adhesion molecules (CAMs) (Zhang et al, 2016; Huang et al, 2018), and the tumor-derived and tumor associated-endothelial cell-derived exosomes uptaken by the organ-specific cells, which prepare the pre-metastatic niche (Hoshino et al. 2015; Zeng et al, 2019).

Dong et al. (2005) experimentally studied the adhesion and migration of human melanoma cells in shear flows using a modified Boyden chamber. Guo et al. (2014) investigated the breast cancer MDA-MB-231 cells arrest and adhesion in rat mesenteric microvasculature *in vivo*. Marshall et al. (2005) used atomic force microscopy to measure the force history during the receptor-ligand dissociation process. Their measurements and analysis emphasized the importance of force application history in deriving the bond off-rates. Microfluidic approaches have also been used for in situ analysis of the single CTC adhesion (Mao et al. 2018). However, due to the complexity of tumor cell adhesion that occurs at nanometer scales, in vivo experimental measurements for the cellular interactions and the forces involved are not available at present. Instead, numerical simulations which can provide much detailed information would be a feasible and valuable tool in exploring the mechanism of cell adhesion under complex flow conditions. Rejniak (2012) studied the effect of deformation of tumor cells on their adhesion in a 2D vessel using the Immersed Boundary model. They examined the parameters related to the structure of the actin network, the cell nucleus and the adhesion links between the tumor and endothelial cells, which enable successful transitions between different transport modes of the adhesion cascade. Xiao et al. (2016a) simulated the adhesion of a CTC in a microvessel using the dissipative particle dynamics (DPD) method, in which the blood was treated as a suspension of red blood cells (RBCs). Since they focused on the effect of the RBC aggregation on the CTC adhesion, a straight vessel geometry was used in their simulations and no curvature effect was taken into consideration. Since most of the CTC adhesion occurred at curvatures (Yan et al. 2010), in this work we investigated the effect of curvature on the CTC adhesion by performing 3D simulations.

Most of the previous experiments and simulations investigated cell adhesions in a straight vessel. Recent in vivo experiments conducted by Liu et al. (2008), Guo et al. (2014) and Zhang et al. (2016) demonstrated that the CTCs prefer to adhere to the curved vessels as well as the bifurcations of the microvasculature. To explore the adhesion mechanism for their observations, Yan et al. (2011; 2010)

numerically investigated the effect of the vessel curvature and wall shear stress on the adhesion of a CTC in a curved vessel. Their results indicate that in the curved vessel, the number of simultaneous bonds increases and thus the adhesion probability. However, their simulation was two-dimensional, and the CTC was simplified to be a rigid disk, which does not reflect the real case as the cell deformability was reported to be closely related to its adhesion activity (Rejniak 2012). Therefore, in the current study, we performed a three-dimensional numerical simulation on the dynamics and adhesion of a deformable CTC in a curved microvessel. The fluid dynamics was solved using DPD. The deformation of the CTC was modeled by a spring-based network membrane model and the CTC adhesion was modeled by a probabilistic adhesive dynamics model.

2. Numerical method and mathematical model

2.1 Dissipative particle dynamics method

The blood flow was simulated by the dissipative particle dynamics (DPD), which is a mesoscopic simulation method frequently adopted in modeling the dynamic and rheological properties of complex fluids (Fan et al. 2006; Soares et al. 2013). In DPD, each particle represents a molecular cluster of mass m_i, position $\boldsymbol{r}_i$, and velocity $\boldsymbol{v}_i$, rather than an individual molecule. The particle interacts with its neighbors through three forces, i.e., a conservative (repulsive) force $\boldsymbol{F}_{ij}^{C}$, a dissipative (friction) force $\boldsymbol{F}_{ij}^{D}$, and a random force $\boldsymbol{F}_{ij}^{R}$. The resultant force $\boldsymbol{F}_i$ exerted on each individual particle is expressed as,

$$\boldsymbol{F}_i = \boldsymbol{F}_e + \sum_{j \neq i} \boldsymbol{F}_{ij}^{C} + \boldsymbol{F}_{ij}^{D} + \boldsymbol{F}_{ij}^{R} \tag{1}$$

where $\boldsymbol{F}_e$ is the external force and the summation includes those neighboring particles j within a cutoff radius r_c. The three interaction forces are calculated respectively as follows,

$$\boldsymbol{F}_{ij}^{C} = \begin{cases} a_{ij}(1 - r_{ij})\hat{\boldsymbol{r}}_{ij}, & for\ r_{ij} \leq r_c \\ 0, & for\ r_{ij} > r_c \end{cases}, \tag{2}$$

$$\boldsymbol{F}_{ij}^{D} = -\gamma \omega^{D}(r_{ij})(\hat{\boldsymbol{r}}_{ij} \cdot \boldsymbol{v}_{ij})\hat{\boldsymbol{r}}_{ij}, \tag{3}$$

$$\boldsymbol{F}_{ij}^{R} = -\sigma \omega^{R}(r_{ij}) \cdot \frac{\xi_{ij}}{\sqrt{dt}} \hat{\boldsymbol{r}}_{ij}, \tag{4}$$

where $\hat{\boldsymbol{r}}_{ij} = \boldsymbol{r}_{ij}/r_{ij}, \boldsymbol{r}_{ij} = \boldsymbol{r}_i - \boldsymbol{r}_j, \boldsymbol{v}_{ij} = \boldsymbol{v}_i - \boldsymbol{v}_j$. a_{ij}, γ, and σ are coefficients for the conservative, dissipative, and random forces, respectively. ξ_{ij} is a random number with zero mean and unit

variance. $\omega^D(r_{ij})$ and $\omega^R(r_{ij})$ are r-dependent weight functions. To satisfy the fluctuation-dissipation theorem in the DPD system, they must hold the relation,

$$\omega^D(r_{ij}) = [\omega^R(r_{ij})]^2 = \begin{cases} \left(1 - \frac{r_{ij}}{r_c}\right)^{1/2}, & for\ r_{ij} \le r_c \\ 0, & for\ r_{ij} > r_c \end{cases}, \qquad \sigma^2 = 2\gamma k_B T \tag{5}$$

For more details of the DPD method, interested readers can refer to (Hoogerbrugge and Koelman 1992). The evolution of the particles is governed by Newton's equations of motion

$$\frac{d\boldsymbol{r}_i}{dt} = \boldsymbol{v}_i, \qquad m_i \frac{d\boldsymbol{v}_i}{dt} = \boldsymbol{F}_i \tag{6}$$

where $m_i = 1$ was assumed. The position $\boldsymbol{r}_i$ and velocity $\boldsymbol{v}_i$ of the particles were advanced by solving the above motion equations using a modified velocity-Verlet algorithm (Espanol and Pep 1995; Groot and Warren 1997).

2.2 Cell membrane model

A spring-based network model is used to simulate the deformation of the elastic cell membrane. The membrane is meshed by a set of triangular elements with the nodes of each element connected by springs. The elastic force on a membrane node *i* can be calculated by

$$\boldsymbol{F}_i^{\text{membrane}} = -\frac{\partial E\{(\boldsymbol{r}_i)\}}{\partial \boldsymbol{r}_i} \tag{7}$$

where $E\{(\boldsymbol{r}_i)\}$ is the total energy of the network and it has four components, i.e.,

$$E\{(\boldsymbol{r}_i)\} = E_{in-plane} + E_{bending} + E_{area} + E_{volume} \tag{8}$$

$E_{in-plane}$ is the in-plane elastic energy. In the WLC-POW model that we adopted, this energy is calculated by

$$E_{in-plane} = \sum_{\text{all edges}} \left(\frac{k_B T l_{max}}{4p} \frac{3x_l - 2x_l^3}{1 - x_l} + \frac{k_p}{(m-1) l^{m-1}} \right) \tag{9}$$

where l_{max} is the maximum spring length allowed, which is 2.2 times the equilibrium spring length in the WLC model (Fedosov et al. 2010). $x_l = l/l_{max}$, where l is the instantaneous spring length. p is the persistence length, k_p is a spring constant in the POW model. k_B is the Boltzmann constant and $T = 310K$ is the temperature of the system. m is a specified exponent and we follow Fedosov et al. (2010) to set it as 2 in our simulations.

The bending energy is defined as,

$$E_{bending} = \sum_{\substack{\text{all triangle} \\ \text{adjacent}}} K_b\left[1 - \cos\left(\theta_{\alpha\beta} - \theta_0\right)\right] \tag{10}$$

where K_b is the bending modulus of the membrane, θ_0 and $\theta_{\alpha\beta}$ are the spontaneous and instantaneous angles between two adjacent elements.

E_{area} and E_{volume} are the energies that account for the conservation constraints of the surface area and volume. They are computed as follows,

$$E_{area} = \frac{K_{area}^{tot}(A^{tot} - A_0^{tot})}{2A_0^{tot}} + \sum_{\text{all triangles}} \frac{K_{area}(A - A_0)^2}{2A_0} \tag{11}$$

$$E_{volume} = \frac{K_{volume}(V^{tot} - V_0^{tot})^2}{2V_0^{tot}} \tag{12}$$

where K_{area}^{tot}, K_{area}, and K_{volume} are the constraint constants for the global cell area, local element area, and cell volume, respectively. A^{tot}, A, and V^{tot} denote the instantaneous global cell area, local element area, and global cell volume, respectively, and their spontaneous values are indexed with "0".

In our simulations, the membrane is assumed to be incompressible and the thickness of the cell is very small. These make the membrane area nearly a constant. To impose such constraint, the value of K_{area}^{tot} is given a relatively large value to conserve the membrane area.

2.3 Cell adhesion model

The adhesion of the CTC to the endothelial cells that form the vessel wall was modeled with a probabilistic model (Hammer and Apte 1992). In this model, the adhesive dynamics is mediated by the interaction between receptors and ligands that exist on the CTC and the endothelial cell, respectively (see Fig.1). The formation and dissociation of a bond between a receptor and a ligand obey the following rule. At each time step, the distance l_b between a receptor and a free ligand is recorded. If this distance is less than the reactive distance d_{on}, a new bond may form with a probability P_{on}. For a preexisting bond, it is ruptured if the distance exceeds a disassociation distance d_{off}. If the distance is below d_{off}, the bond has a probability of P_{off} to be ruptured or left unchanged otherwise. P_{on} and P_{off} can be expressed as

$$P_{\text{on}} = \begin{cases} 1 - e^{-k_{\text{on}}\Delta t}, & l_b < d_{\text{on}} \\ 0, & l_b \geq d_{\text{on}} \end{cases} \tag{13}$$

$$P_{\text{off}} = \begin{cases} 1 - e^{-k_{\text{off}}\Delta t}, & l_b < d_{\text{off}} \\ 1, & l_b \geq d_{\text{off}} \end{cases} \tag{14}$$

where Δt is the time step size, k_{on} and k_{off} are the association (on) and dissociation (off) rates and they can be computed as,

$$k_{\text{on}} = k_{\text{on}}^0 \exp\left(-\frac{\sigma_{\text{on}}(l_b - l_b^0)^2}{2k_B T}\right) \tag{15}$$

$$k_{\text{off}} = k_{\text{off}}^0 exp\left(\frac{\sigma_{\text{off}}(l_b - l_b^0)^2}{2k_B T}\right) \tag{16}$$

where k_{on}^0 and k_{off}^0 are the unstressed "on" and "off" rates when the distance l_b equals to the equilibrium spring length l_b^0. σ_{on} and σ_{off} are effective "on" and "off" strengths. If a bond exists, a spring force F_s along the receptor and ligand link would be generated to force the CTC to adhere to the vessel wall.

$$F_s(l_b) = K_s(l_b - l_b^0) \tag{17}$$

where K_s is the spring constant.

To determine the state of the bond, a stochastic Monte Carlo technique was introduced in this study. That is, for each bond within the effective distance d_{on} or d_{off}, two uniformly distributed random numbers ξ_1 and $\xi_2 \in [0, 1]$ would be generated. A bond would form when $P_{\text{on}} > \xi_1$, and an existing bond would rupture when $P_{\text{off}} > \xi_2$.

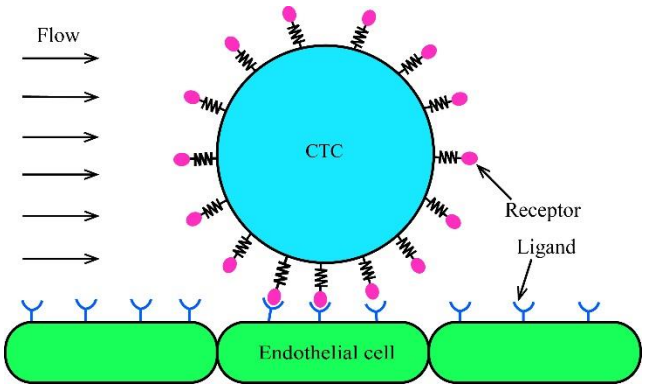

Fig.1 Schematic diagram of the adhesion model

3. Results and discussion

3.1 Physical model and simulation parameters

The simulations were three-dimensional and the cell membrane of the CTC was considered to be elastic. The cytoplasm enclosed by the membrane was also modeled as a DPD fluid that has the same property of the blood plasma. The geometry of the curved vessel we considered is the same as that of Yan et al. (2010) (but in three-dimensional), which is depicted in Fig.2. The microvessel was assumed to be left-right symmetrical and curved at its middle section with smooth transitions. The origin of the coordinate system is located at O, and for an easier description of the adhesion sites, the curved section is divided into three bends, as shown in the figure. A CTC with a spherical shape of diameter d_c is released at the straight section of the vessel with an initial vertical position H_0. In our simulations, the flow is driven by a constant azimuthal body force density $\boldsymbol{f}_d$ which is a substitution of the pressure gradient. For convenience, the flow was assumed periodic along the y-direction, and the vessel wall was assumed to be rigid and impermeable, thus it is imposed with the no-slip boundary condition. Unless otherwise stated, the basic parameters involved in our simulations are listed in Table 1, where a length scaling factor $C_l = 1 \times 10^{-6}$m, a viscosity scaling factor $C_\mu = 5.1 \times 10^{-5}$Pa·s, and an energy scaling factor $C_e = 4.28 \times 10^{-21}$J were used. The validation of the hybrid method and the numerical code was conducted in our previous studies (Xiao et al. 2014; Xiao et al. 2016b; Xiao et al. 2016c).

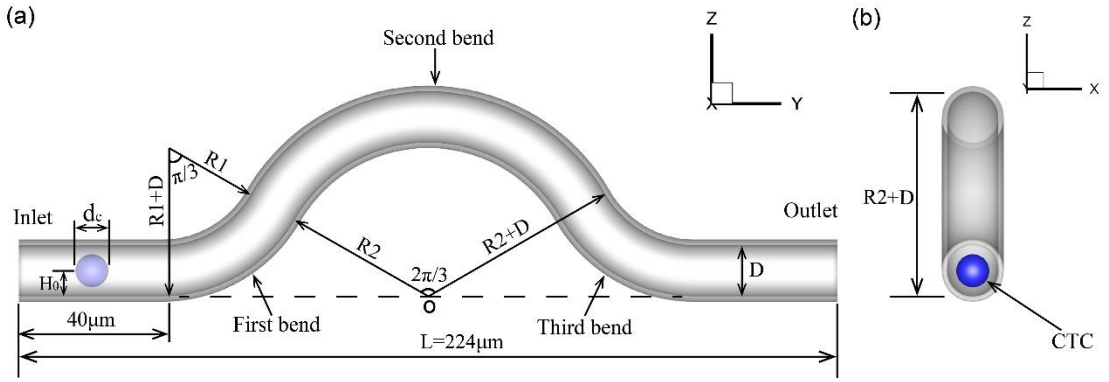

Fig.2 The geometry of the curved vessel (a) front view (b) side view

Table 1 Basic parameters used in the simulations

Parameters	Physical value	Simulation input
CTC diameter (d_c)	9μm	9
Vessel diameter (D)	14μm	14
Radius $R1$	28μm	28

Radius $R2$	42μm	42
Initial vertical position (H_0)	7μm	7
Blood plasma viscosity (μ)	1.2×10^{-3}Pa · s (Skalak and Chien 1987)	1.43
k_BT (where $T = 310$K)	4.28×10^{-21}J	1
Driven force density (f)	1.284×10^{5}N/m^3	30
Membrane bending modulus (K_b)	3.6×10^{-18}J (Fedosov et al. 2010)	841.12
Global area constraint constant (K_{area}^{tot})	3.35×10^{-3}N/m (Xiao et al. 2016a)	7.83×10^{5}
Local area constraint constant (K_{area})	5.2×10^{-6}N/m (Xiao et al. 2016a)	1.21×10^{3}
Volume constraint constant (K_{volume})	3.35×10^{-3}N/m (Xiao et al. 2016a)	7.83×10^{5}
Unstressed on rate (k_{on}^0)	1×10^{4}s^{-1} (Schwarz and Alon 2004)	1960
Unstressed off rate (k_{off}^0)	$20s^{-1}$ (Alon 1997)	3.92
Effective on strength (σ_{on})	5×10^{-7}N/m (Dembo et al. 1988)	116.82
Effective off strength (σ_{off})	5×10^{-8}N/m (Dembo et al. 1988)	11.68
Association distance (d_{on})	0.1μm	0.1
Disassociation distance (d_{off})	0.1μm	0.1
Spring constant (K_s)	2×10^{-3}N/m (Chang and Hammer 1996)	4.67×10^{5}
Equilibrium spring length (l_b^0)	0.025μm (Dembo et al. 1988)	0.025
Receptor density (n_r)	4.63/μm^2	4.63
Ligand density (n_l)	1.73/μm^2	1.73
Time step (Δt)	4.9×10^{-5}s	2.5×10^{-4}
Cut off radius (r_c)	1.0μm	1.0
coefficients for the conservative force (a_{ij})	/	25
Coefficient for dissipative force (γ) for the blood	/	4.5

3.2 CTC adhesion in straight and curved vessels

We first simulated the adhesion of a CTC respectively in a curved and a straight vessel and characterized the difference. Note that the length of the straight vessel is equal to that of the curved one (i.e. a CTC travels the the same distance from the inlet to the outlet of a vessel) and all the other simulation parameters are identical. The evolutions of the CTC in the curved and straight vessels are shown in Fig. 3a and Fig. 3b, respectively, where both the front and top views are presented and

those cell-wall contact areas are highlighted in yellow. We can see that the CTC gradually gets deformed as it migrates to the downstream of the vessel in both curved and straight vessels. Multiple cell-wall contacts can be observed in the curved vessel while the contact occurs only once in the straight vessel. The contacts in the curved vessel are very likely caused by the centrifugal force as the CTC is observed to move outward, away from the center of curvature. A typical unsuccessful adhesion process observed in the curved vessel is shown in Fig. 3c. When the CTC collides the vessel inner wall, the reaction force from the wall flattens part of the cell membrane, resulting in an increased contact surface area. This promotes the formation of bonds as more receptors will be within the reactive distance d_{on}. When the bonds are formed, the accompanying adhesive spring force will drag the cell and prevent it from escaping that site (cell arrest). The anti-adhesive force (e.g. the hydrodynamic force and the reaction force from the wall), on the contrary, suppresses this arrest action. The competition between the anti-adhesive and adhesive forces decides the stay or departure of the CTC. Once the anti-adhesive force dominates, as in this simulated case, the CTC will keep moving forward and a spike is formed due to the adhesive drag force. As the CTC departs further from this site, all the bonds will get ruptured and the CTC will eventually escape the arrest and recover to a spherical shape.

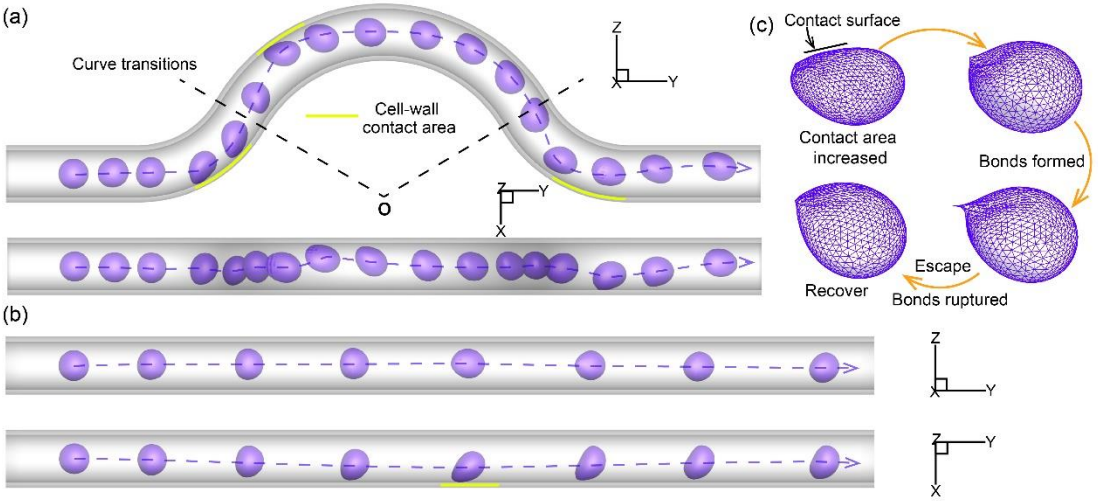

Fig. 3 The evolution of the CTC in a curved vessel (a) and in a straight vessel (b). A typical unsuccessful adhesion process observed in the curved vessel (c).

The three-dimensional trajectories of the center of the CTC in the curved and straight vessels are shown in Fig. 4a and Fig. 4b, respectively. We can see that the CTC does not travel exactly along the vessel axis and its trajectory in each vessel is not even in the same plane. Compared with the straight vessel case, the trajectory of the CTC in the curved vessel case deviates more from the vessel axis due to the centrifugal effect, forcing the CTC closer to the vessel wall during its migration. Once the receptors of the CTC and the ligands on the wall are within the association distance, bonds may be formed and the induced adhesive forces will further pull the CTC toward the vessel wall and possibly cause cell-wall contacts. This may be the reason why in our relatively low-*Re* flow in a microvessel, where viscous effect dominates, the cell-wall contacts are possible in the curved vessel case.

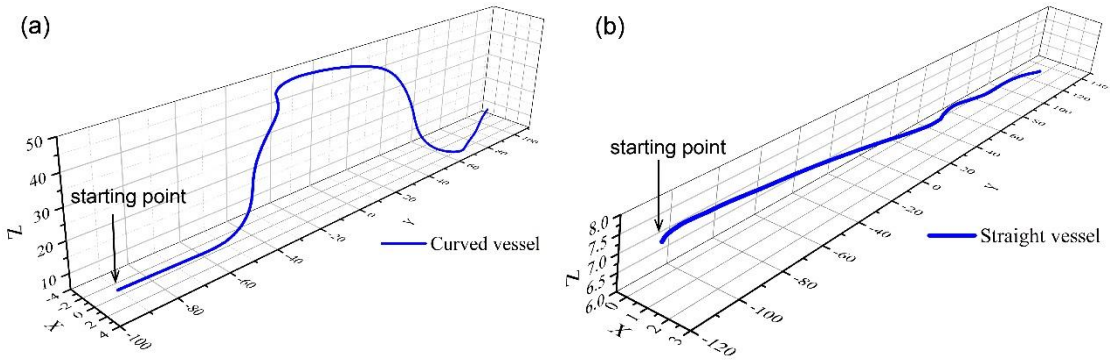

Fig. 4 Trajectories of the center of CTC in the curved (a) and straight (b) vessels

Figure 5a shows the time evolution of the velocity magnitude of a CTC. The evolution curve of the CTC's vertical position (dash-dot-dash line) in the curved vessel is also presented as a reference for its location. It can be seen from the figure that the CTC in the straight vessel travels much faster than that in the curved vessel as the time spent for migrating over the entire length of the vessel is nearly doubled in the curved vessel. The difference in the cell velocity magnitude is not apparent initially until the CTC in the curved vessel enters the first bend of the vessel. Since then its velocity magnitude fluctuates around the value of 0.1mm/s for the rest of the journey. On the contrary, the CTC in the straight vessel keeps accelerating from the beginning of the journey, although there is an ephemeral fluctuation in the velocity magnitude in the middle of the journey. This is likely caused by the cell-wall contact (Fig. 3b). The multiple fluctuations in the cell velocity magnitude for the

curved vessel can be attributed to the cell-wall contacts and the adhesion effect, as their occurring locations correspond with each other (Figs. 3a and 5a). The time evolutions of the number of bonds formed in the curved and straight vessels are shown in Fig. 5c-d. In the curved vessel, intensive bond formations can be observed at three different sites with a maximum bond number of 7 (i.e. a functional receptor density of 0.0276/ um^2 and roughly 0.6% of the receptors bound to the ligands), while no bonds are formed at all in the straight vessel, indicating that the curvature of the vessel plays a significant role in the CTC adhesion. Interestingly, in the curved vessel the bond formation occurs more around the transition region (the locations where vessel curvature starts to vary) of the curved part, where cell-wall contacts are also more prevalent (see Fig. 3a). A statistical analysis on the probability to form bonds at a specified number in the curved and straight vessels are shown in Fig. 5b, where we can see that although the probability of the bond formation in the curved vessel is low (<10%), it is still much higher than that in the straight vessel (almost zero). Since the probability of the bond formation also depends on the receptor and ligand densities, for the densities chosen in the current study, it is at the low end, which may reflect the real situation that the arrest and adhesion of the CTCs do not happen frequently.

To describe the deformation of the CTC, the time evolutions of the volume and surface area of the CTC are recorded and plotted in Fig. 6a and Fig. 6b, respectively. It is found that when the CTC contacts the wall, its volume slightly decreases (< 4%) while its surface area slightly increases (< 6%, as we use a large K_{area}^{tot} in simulations). That is why several slumps in the volume and leaps in the surface area can be observed in the curved vessel case. The shrinkage of the cell volume helps to reduce the hydrodynamic force exerted on the cell, while the expansion in the cell surface area enables a more comprehensive contact. Such an adjustment on the membrane configuration could increase the chance for the successful adhesion.

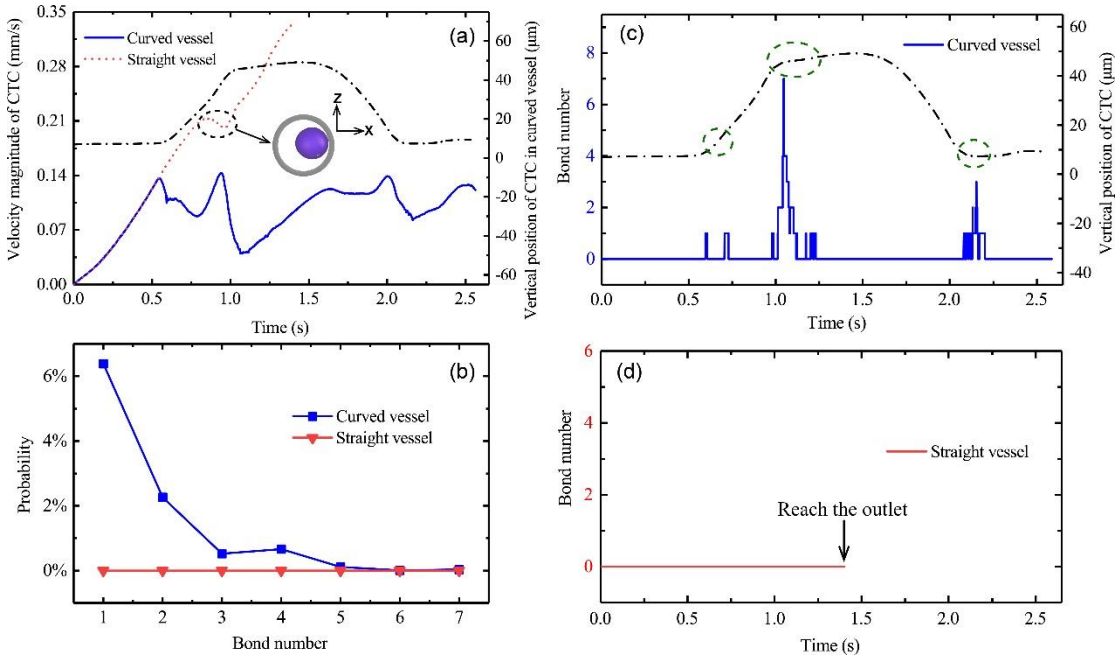

Fig. 5 The time evolutions of the velocity magnitude of a CTC (a), the probability to form bonds at a specified number (b), and the number of bonds formed in the curved (c) and straight (d) vessels. The dash-dot-dash line in (a) and (c) represents the vertical position of the CTC with the scale shown at the right axis.

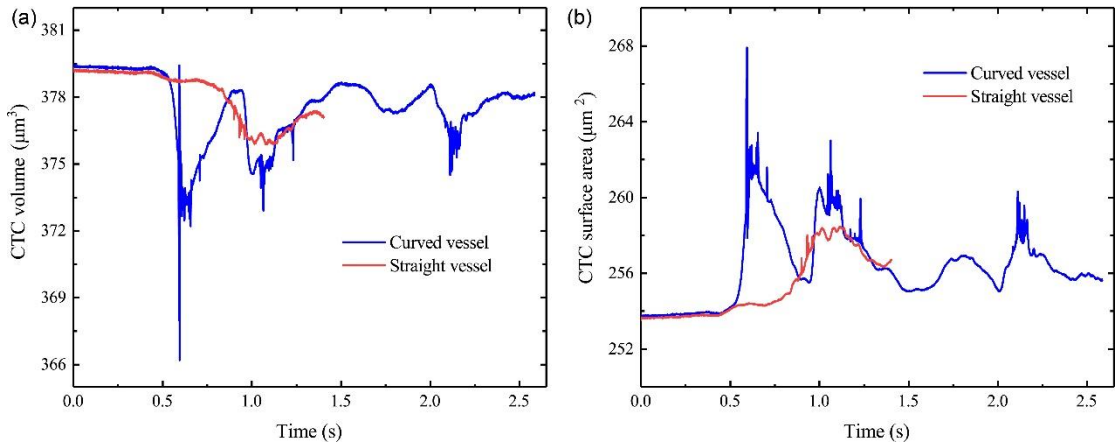

Fig. 6 The time evolution of the volume (a) and surface area (b) of a CTC in the curved and straight vessels

3.3 Effect of driven force density on the CTC adhesion

To explore the effect of the applied driven force density *f* (or the flow Reynolds number) on the cell dynamics and adhesion, we ran more simulation cases in which the applied *f* was chosen as 15, 30

and 45, respectively. Figures 7a-c show the time evolutions of the bond number at different values of *f* and Fig. 7d shows the probability to form bonds at a specified number for each case. It is observed that both of the average bond number and the bond formation probability increase with the applied *f*. When *f*=15, bond formation occurs only at two sites of the vessel and the bond number is quite limited in terms of the maximum and average values (3 and 0.0658, respectively). When *f*=30, bond formation occurs at three sites and the bond number reaches an average of 0.159 and a maximum of 7, respectively. When the applied *f* increases further to 45, the bond number reaches to 0.191 on average, and the bond formation occurs at four sites of the vessel wall, one site even in the straight section at downstream. This is expected, as when a larger value of *f* is applied, the cell's velocity magnitude increases (see the velocity magnitude of the CTC as a function of the y-coordinate of the cell center in Fig. 7e), resulting in a larger centrifugal force on the cell. The increased centrifugal force, as discussed in Section 3.2, would cause the CTC to deviate from the vessel axis and enhance the possibility of cell-wall contacts. However, it should be noted that the increase in the number of the bonds formed and that in the cell adhesion possibility shall not be simply considered as equivalent, as the increased driven force density also brings a larger hydrodynamic force (part of the anti-adhesive force) that tends to facilitate the escape of the CTC from the arrest mode by the formed bonds. Another feature can also be observed in Fig. 7a-c, that is, when the applied *f* is small, as in the case of *f*=15, the most active site for the bond formation is located at the first bend of the vessel. However, as the value of *f* exceeds a certain threshold (e.g., 30), the cell is more likely to form bonds at the left half of the second bend of the curved vessel, even at the third bend.

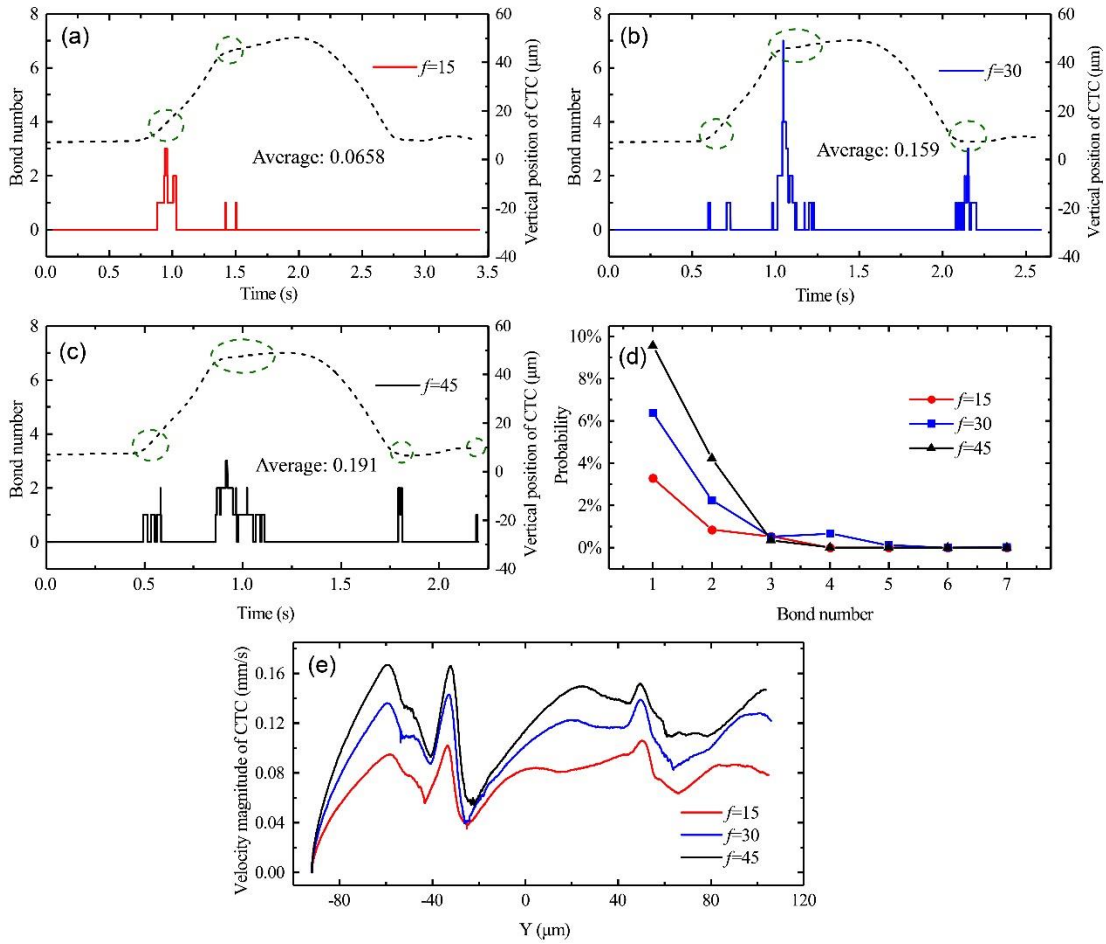

Fig. 7 The time evolutions of the bond number at f=15 (a), f=30 (b) and f=45 (c), the probability to form bonds at a specified number (d) and the velocity magnitude of a CTC as a function of the y-coordinate of the cell center (e). The short-dashed line in (a-c) represents the vertical position of the CTC with the scale shown at the right axis.

3.4 Effect of the membrane bending modulus on CTC adhesion

The effect of the membrane bending modulus K_b on CTC adhesion was investigated by simulating an extra case on the migration of a softer CTC ($K_b = 500$) in the same curved vessel at f=15. The results were compared with those in the prior case when $K_b = 841.12$. The time evolutions of the cell's velocity magnitude are shown in Fig. 8a, where little difference can be observed. This indicates that the membrane bending modulus will not significantly influence the velocity magnitude of CTC. Figures 8c-d show the time evolutions of the number of bonds formed when $K_b = 500$ and 841.12, respectively. We can see that the K_b of the CTC plays a significant role in

the bond formation and thus cell adhesion. It is observed that when the K_b of CTC is reduced by 40%, from 841.12 to 500, the average number of the bonds formed increases from 0.0658 to 0.134 (nearly by 104%). Figure 9a shows the probability to form bonds at a specified number for the cases when $K_b = 500$ and 841.12. We can see that the probability increases remarkably when K_b decreases from 841.12 to 500, suggesting that the softer a CTC is, the more adhesive it is to the vessel wall. By looking at the time evolution of the CTC surface area in Fig. 8b, one can see that every cell-wall contact induces a leap in the surface area of CTC. The leaps become more severe in the softer CTC case. The increased surface areas at these leaps enable more comprehensive cell-wall contacts, as explicitly shown in Fig. 9b. Apart from the increase in the number of bonds formed, it is also observed from Figs. 8c-d that bonds are formed intensively at four sites of the vessel in the softer CTC case while only two sites are found in the stiffer CTC case. This difference is out of our expectation before the simulation. Furthermore, the most active bond formation site is found to be relocated to the left half of the second bend of the vessel, may be the third bend as well.

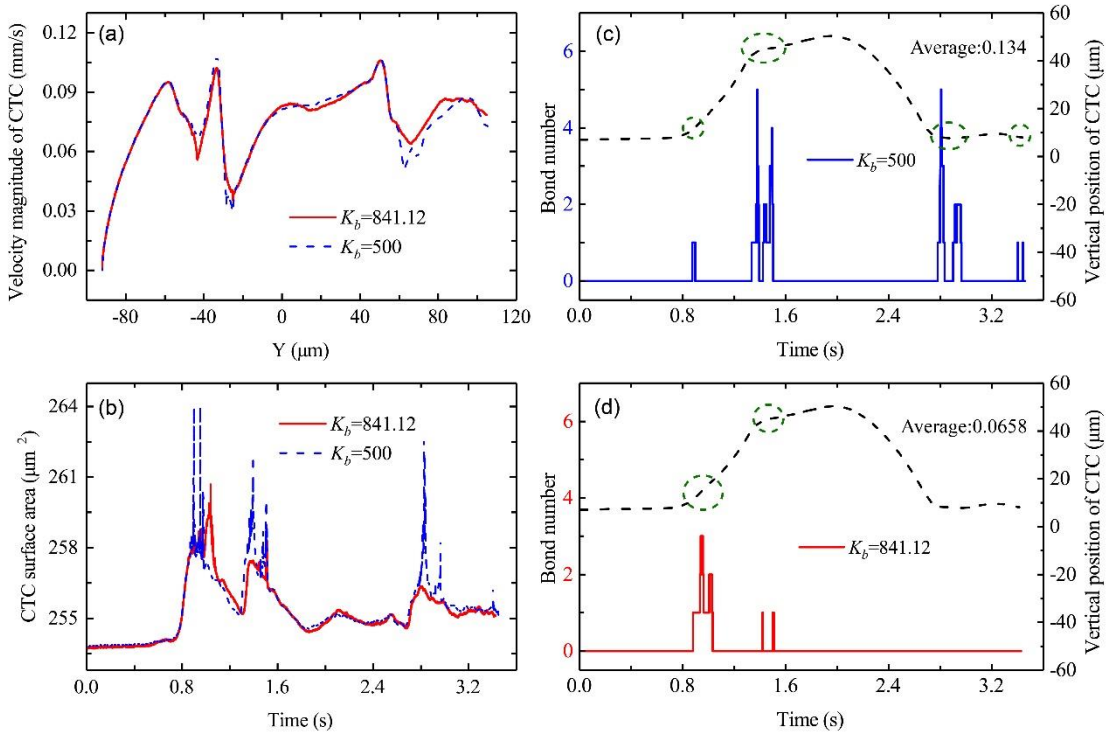

Fig. 8 The velocity magnitude of CTC as a function of the y-coordinate of the cell center (a), and the time evolution of the CTC surface area (b), and the number of bonds formed when $K_b = 500$ (c) and $K_b = 841.12$ (d). The dashed line in (c-d) represents the vertical position of the CTC with the scale shown at the right axis.

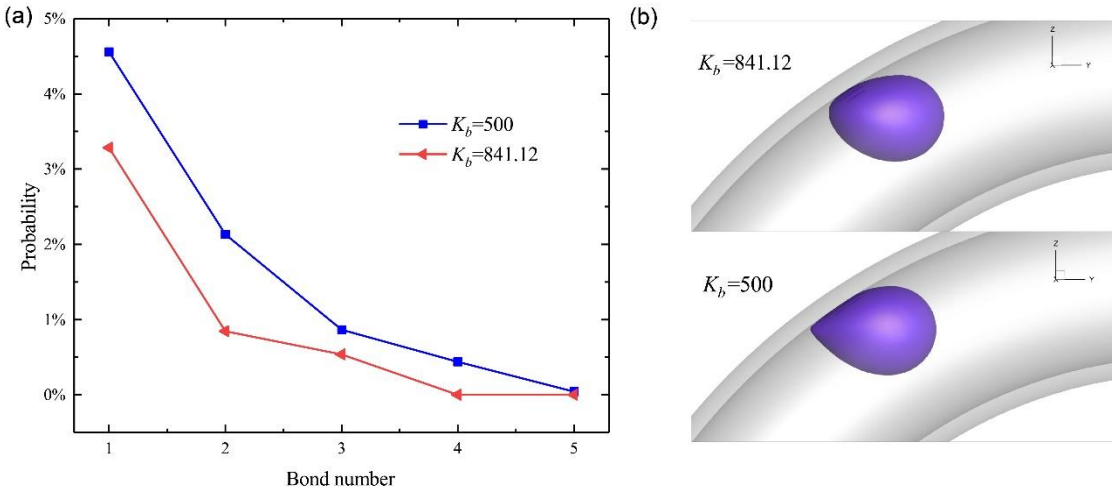

Fig. 9 The probability to form bonds at a specified number (a) and a comparison of the cell-wall contact at the second bend of the vessel with each snapshot taken when a full-contact happens (b)

3.5 Limitations and future studies

One limitation in our present model is that it can only simulate the adhesion of a single CTC in a blood vessel. The effects of other cells, such as the red blood cells (RBCs), leukocytes, and platelets, on the CTC adhesion cannot be investigated unless extra models are incorporated into the current model to handle cell-cell interactions and RBC aggregability. Another limitation is that our current model is unable to include the effect of the vessel elasticity on the CTC adhesion. These limitations will be overcome in the future to make the model more versatile and robust.

The present study is an initial step towards the investigation on the CTC adhesion in the real microvasculature with the complicated geometric patterns. We list here some future studies that will follow the research described in the current study. One is to explore the influence of the circulating blood cells on the CTC adhesion. As blood is a concentrated suspension containing a variety of cells, the blood cells (e.g. RBCs, leukocytes and platelets) certainly should play an important role in the transport and adhesion of the CTCs. Apart from that, a number of studies have observed clusters of the CTCs in the circulation (King et al. 2015; Phillips et al. 2015). How will the CTC clusters respond in a curved vessel? Will the CTC clusters facilitate or inhibit the CTC adhesion compared with the single cell case? Further research is required to answer these questions. Since tumor cells have their specific metastatic organs, e.g., colon cancer preferentially metastasizes to the liver

(Mook et al, 2003), and the cell adhesion molecules (receptors and ligands) can be activated by both mechanical (e.g., blood flow) and chemical (e.g., cytokines) stimuli (Wirtz et al, 2011; Zhang et al, 2016; Huang et al, 2018), a model with the spatio-temporal distributions for the receptors and ligands, as well as the varied kinetics for the bond formation, will be developed to reflect the local mechanochemical factors in the specific organ on the CTC adhesion and transmigration. Some other relevant factors can also be investigated, such as vessel geometry types (e.g. bifurcated vessels) and sizes, as well as the initial position of the CTCs.

4. Conclusions

In this study, the adhesion of a CTC in a curved microvessel was numerically investigated using a hybrid method that integrates the DPD method, the spring-based network model, and the probabilistic adhesion model. The dynamics and adhesion of a CTC in both straight and curved vessels with an equal length were first investigated and the differences were characterized. After that, a parametric study was performed to explore the effects of the driven force density f and the membrane bending modulus K_b on the CTC adhesion. Based on our simulation results, the following conclusions can be drawn:

1. A CTC is more likely to adhere to a curved vessel as more bonds will be formed around the transition region of the curved vessel due to the centrifugal force which deviates the motion of the CTC from the vessel axis and causes CTC-wall contacts. Compared with that in the straight vessel, the cell's velocity magnitude in the curved vessel is much smaller and more fluctuant due to the CTC-wall contact and the adhesion effect.
2. Increasing the applied f or decreasing the K_b promote bond formations and outspread the bond formation sites in the curved vessel. The former brings a larger centrifugal force while the latter increases the contact surface area during CTC-wall contacts, both are beneficial to the bond formation. Apart from that, the most active site for bond formations in a curved vessel also varies with the applied f and the K_b. For our vessel geometry, it is found that, when f is small, the most active site for bond formation is located at the first bend of the vessel. However, as f increases or K_b decreases, the site where the most bonds are formed shifts to the left half of the second bend of the vessel.

Acknowledgments

The authors appreciate the valuable comments from the anonymous referees. The support given by the Hong Kong Polytechnic University under grant Nos. G- UACM and G-UAHL, and Shanghai Sailing Program under grant No. 19YF1417400, and National Natural Science Foundation of China under grant No. 11902188 is gratefully acknowledged.

Conflicts of Interest

The authors declare that they do not have any Conflict of Interest.

References

Alon R (1997) The Kinetics of L-selectin Tethers and the Mechanics of Selectin-mediated Rolling Journal of Cell Biology 138:1169-1180

Bao, G., Kamm, R.D., Thomas, W. *et al.* Molecular Biomechanics: The Molecular Basis of How Forces Regulate Cellular Function. *Cel. Mol. Bioeng.* **3,** 91–105 (2010). https://doi.org/10.1007/s12195-010-0109-z

Cai B, Fan J, Zeng M, Zhang L, Fu BM. Adhesion of malignant mammary tumor cells MDA-MB-231 to microvessel wall increases microvascular permeability via degradation of endothelial surface glycocalyx. *J Appl Physiol.* 2012;113(7):1141-1153. doi:10.1152/japplphysiol.00479.2012

Chang K-C, Hammer D (1996) Influence of Direction and Type of Applied Force on the Detachment of Macromolecularly-Bound Particles from Surfaces Langmuir 12 doi:10.1021/la950690y

Dembo M, Torney D, Saxman K, Da H (1988) The Reaction-Limited Kinetics of Membrane-to-Surface Adhesion and Detachment Proceedings of the Royal Society of London

Series B, Containing papers of a Biological character Royal Society (Great Britain) 234:55-83 doi:10.1098/rspb.1988.0038

Dong C, Slattery M, Liang S (2005) Micromechanics of tumor cell adhesion and migration under dynamic flow conditions Frontiers in bioscience : a journal and virtual library 10:379-384

Espanol, Pep (1995) Hydrodynamics from dissipative particle dynamics Phys Rev E Stat Phys Plasmas Fluids Relat Interdiscip Topics 52:1734-1742

Fan X, Phan-Thien N, Chen S, Wu X, Yong Ng T (2006) Simulating flow of DNA suspension using dissipative particle dynamics Physics of Fluids 18:063102

Fedosov DA, Caswell B, Karniadakis GE (2010) Systematic coarse-graining of spectrin-level red blood cell models Computer Methods in Applied Mechanics and Engineering 199:1937-1948 doi:https://doi.org/10.1016/j.cma.2010.02.001

Groot RD, Warren PB (1997) Dissipative particle dynamics: Bridging the gap between atomistic and mesoscopic simulation The Journal of Chemical Physics 107:4423-4435 doi:10.1063/1.474784

Guo P, Cai B, Lei M, Liu Y, Fu BM (2014) Differential arrest and adhesion of tumor cells and microbeads in the microvasculature Biomechanics and Modeling in Mechanobiology 13:537-550

Haier J, Nicolson G (2001) Haier J, Nicolson GL.. Tumor cell adhesion under hydrodynamic conditions of fluid flow. APMIS 109: 241-262 APMIS : acta pathologica, microbiologica, et immunologica Scandinavica 109:241-262 doi:10.1034/j.1600-0463.2001.d01-118.x

Hammer DA, Apte SM (1992) Simulation of cell rolling and adhesion on surfaces in shear flow: general results and analysis of selectin-mediated neutrophil adhesion Biophysical Journal 63:35-57 doi:https://doi.org/10.1016/S0006-3495(92)81577-1

Hoogerbrugge PJ, Koelman JMVA (1992) Simulating Microscopic Hydrodynamic Phenomena with Dissipative Particle Dynamics Europhysics Letters (EPL) 19:155-160

Hoshino A et al. (2015) Tumour exosome integrins determine organotropic metastasis Nature 527 doi:10.1038/nature15756

Huang Q, Hu X, He W, et al. Fluid shear stress and tumor metastasis. *Am J Cancer Res*. 2018;8(5):763-777.

Janiszewska M, Primi M, Izard T (2020) Cell adhesion in cancer: Beyond the migration of single cells Journal of Biological Chemistry 295:jbc.REV119.007759 doi:10.1074/jbc.REV119.007759

King MR et al. (2015) A physical sciences network characterization of circulating tumor cell aggregate transport American Journal of Physiology-Cell Physiology 308:C792-C802 doi:10.1152/ajpcell.00346.2014

Liu Q, Mirc D, Fu BM (2008) Mechanical mechanisms of thrombosis in intact bent microvessels of rat mesentery Journal of Biomechanics 41:2726-2734 doi:https://doi.org/10.1016/j.jbiomech.2008.06.013

Mao S, Zhang Q, Haifeng L, Zhang W, Huang Q, Khan M, Lin J-M (2018) Adhesion analysis of single circulating tumor cell on base layer of endothelial cells using open microfluidics Chemical Science 9 doi:10.1039/C8SC03027H

Marshall B, Sarangapani K, Lou J, McEver R, Zhu C (2005) Force History Dependence of Receptor-Ligand Dissociation Biophysical journal 88:1458-1466 doi:10.1529/biophysj.104.050567

Mook OR, Van Marle J, Vreeling-Sindelárová H, Jonges R, Frederiks WM, Van Noorden CJ. Visualization of early events in tumor formation of eGFP-transfected rat colon cancer cells in liver. *Hepatology*. 2003;38(2):295-304. doi:10.1053/jhep.2003.50297

Phillips KG et al. (2015) The thrombotic potential of circulating tumor microemboli: computational modeling of circulating tumor cell-induced coagulation American Journal of Physiology-Cell Physiology 308:C229-C236 doi:10.1152/ajpcell.00315.2014

Poudineh M et al. (2016) Profiling Functional and Biochemical Phenotypes of Circulating Tumor Cells Using a Two-Dimensional Sorting Device Angewandte Chemie International Edition doi:10.1002/ange.201608983

Rejniak KA (2012) Investigating dynamical deformations of tumor cells in circulation: predictions from a theoretical model Frontiers in oncology 2:111 doi:10.3389/fonc.2012.00111

Schwarz U, Alon R (2004) From The Cover: L-selectin-mediated leukocyte tethering in shear flow is controlled by multiple contacts and cytoskeletal anchorage facilitating fast rebinding events Proceedings of the National Academy of Sciences of the United States of America 101:6940-6945 doi:10.1073/pnas.0305822101

Skalak R, Chien S (1987) Handbook of bioengineering. McGraw-Hill, New York

Soares J, Gao C, Alemu Y, Slepian M, Bluestein D (2013) Simulation of Platelets Suspension Flowing Through a Stenosis Model Using a Dissipative Particle Dynamics Approach Annals of biomedical engineering 41 doi:10.1007/s10439-013-0829-z

Weiss L (1990) Invivo Selection of Human Renal-Carcinoma Cells with High Metastatic Potential in Nude-Mice - Comments Clin Exp Metastas 8:103-106 doi:Doi 10.1007/Bf00155596

Weiss L (1992) Biomechanical Interactions of Cancer-Cells with the Microvasculature during Hematogenous Metastasis Cancer and Metastasis Reviews 11:227-235 doi:Doi 10.1007/Bf01307179

Wirtz D, Konstantopoulos K, Searson PC (2011) The physics of cancer: the role of physical interactions and mechanical forces in metastasis Nature reviews Cancer 11:512-522 doi:10.1038/nrc3080

Xiao L, Chen S, Lin C, Liu Y (2014) Simulation of a Single Red Blood Cell Flowing Through a Microvessel Stenosis Using Dissipative Particle Dynamics Molecular & cellular biomechanics : MCB 11:67-85

Xiao L, Liu Y, Chen S, Fu B (2016a) Effects of flowing RBCs on adhesion of a circulating tumor cell in microvessels Biomechanics and Modeling in Mechanobiology 16 doi:10.1007/s10237-016-0839-5

Xiao L, Liu Y, Chen S, Fu B (2016b) Numerical simulation of a single cell passing through a narrow slit Biomechanics and Modeling in Mechanobiology 15 doi:10.1007/s10237-016-0789-y

Xiao L, Liu Y, Chen S, Fu B (2016c) Simulation of Deformation and Aggregation of Two Red Blood Cells in a Stenosed Microvessel by Dissipative Particle Dynamics Cell Biochemistry and Biophysics 74 doi:10.1007/s12013-016-0765-2

Yan W, Cai B, Liu Y, Fu B (2011) Effects of wall shear stress and its gradient on tumor cell adhesion in curved microvessels Biomechanics and modeling in mechanobiology 11:641-653 doi:10.1007/s10237-011-0339-6

Yan W, Liu Y, Fu B (2010) Effects of curvature and cell-cell interaction on cell adhesion in microvessels Biomechanics and modeling in mechanobiology 9:629-640 doi:10.1007/s10237-010-0202-1.

Zeng Y, Yao X, Liu X, et al. Anti-angiogenesis triggers exosomes release from endothelial cells to promote tumor vasculogenesis. *J Extracell Vesicles*. 2019;8(1):1629865. Published 2019 Jun 17. doi:10.1080/20013078.2019.1629865

Zhang L, Zeng M, Fu B (2016) Inhibition of endothelial nitric oxide synthase decreases breast cancer cell MDA-MB-231 adhesion to intact microvessels under physiological flows American journal of physiology Heart and circulatory physiology 310:ajpheart.00109.02016 doi:10.1152/ajpheart.00109.2016

Zhu C, Bao G, Wang N (2000) Cell mechanics: Mechanical response, cell adhesion, and molecular deformation Annu Rev Biomed Eng 2:189-226 doi:DOI 10.1146/annurev.bioeng.2.1.189